

Assessment of Perfused Foveal Microvascular Density and Identification of Nonperfused Capillaries in Healthy and Vasculopathic Eyes

Alexander Pinhas,^{1,2} Moataz Razeen,^{1,3} Michael Dubow,^{1,2} Alexander Gan,¹ Toco Y. Chui,^{1,2} Nishit Shah,¹ Mitul Mehta,¹ Ronald C. Gentile,^{1,4} Rishard Weitz,¹ Joseph B. Walsh,¹ Yusufu N. Sulai,⁵ Joseph Carroll,⁶⁻⁹ Alfredo Dubra,⁶⁻⁸ and Richard B. Rosen^{1,2}

¹Department of Ophthalmology, New York Eye and Ear Infirmary of Mount Sinai, New York, New York, United States

²Icahn School of Medicine at Mount Sinai, New York, New York, United States

³Alexandria Faculty of Medicine, University of Alexandria, Alexandria, Egypt

⁴Department of Ophthalmology, Winthrop-University Hospital, Mineola, New York, United States

⁵The Institute of Optics, University of Rochester, Rochester, New York, United States

⁶Department of Ophthalmology, Medical College of Wisconsin, Milwaukee, Wisconsin, United States

⁷Department of Biomedical Engineering, Marquette University, Milwaukee, Wisconsin, United States

⁸Department of Biophysics, Medical College of Wisconsin, Milwaukee, Wisconsin, United States

⁹Department of Cell Biology, Neurobiology, and Anatomy, Medical College of Wisconsin, Milwaukee, Wisconsin, United States

Correspondence: Richard B. Rosen, New York Eye and Ear Infirmary of Mount Sinai, 310 E 14th Street, New York, NY 10004, USA; rrosen@nyee.edu.

AP and MR contributed equally to the work presented here and therefore should be regarded as joint first authors.

Submitted: June 30, 2014

Accepted: November 3, 2014

Citation: Pinhas A, Razeen M, Dubow M, et al. Assessment of perfused foveal microvascular density and identification of nonperfused capillaries in healthy and vasculopathic eyes. *Invest Ophthalmol Vis Sci.* 2014;55:8056-8066. DOI:10.1167/iovs.14-15136

PURPOSE. To analyze the foveal microvasculature of young healthy eyes and older vasculopathic eyes, imaged using *in vivo* adaptive optics scanning light ophthalmoscope fluorescein angiography (AOSLO FA).

METHODS. AOSLO FA imaging of the superficial retinal microvasculature within an 800- μm radius from the foveal center was performed using simultaneous confocal infrared (IR) reflectance (790 nm) and fluorescence (488 nm) channels. Corresponding IR structural and FA perfusion maps were compared with each other to identify nonperfused capillaries adjacent to the foveal avascular zone. Microvascular densities were calculated from skeletonized FA perfusion maps.

RESULTS. Sixteen healthy adults (26 eyes; mean age 25 years, range, 21–29) and six patients with a retinal vasculopathy (six eyes; mean age 55 years, range, 44–70) were imaged. At least one nonperfused capillary was observed in five of the 16 healthy nonfellow eyes and in four of the six vasculopathic eyes. Compared with healthy eyes, capillary nonperfusion in the vasculopathic eyes was more extensive. Microvascular density of the 16 healthy nonfellow eyes was $42.0 \pm 4.2 \text{ mm}^{-1}$ (range, 33–50 mm^{-1}). All six vasculopathic eyes had decreased microvascular densities.

CONCLUSIONS. AOSLO FA provides an *in vivo* method for estimating foveal microvascular density and reveals occult nonperfused retinal capillaries. Nonperfused capillaries in healthy young adults may represent a normal variation and/or an early sign of pathology. Although limited, the normative data presented here is a step toward developing clinically useful microvascular parameters for ocular and/or systemic diseases.

Keywords: adaptive optics, scanning light ophthalmoscopy, fluorescein angiography, retinal microvasculature, image analysis

Pathological changes in the retinal vasculature, such as arteriolar narrowing and arteriovenous nicking, have been shown to be independent risk factors for increased morbidity and mortality from cardiovascular disease.^{1–6} Histologic studies of human and animal retinas have identified capillary nonperfusion as an important feature of various vaso-occlusive diseases, including diabetes, hypertension, and sickle cell disease.^{7–14} Capillary closure is thought to be an early pivotal event leading to impaired perfusion and ischemia, a cause of irreversible tissue damage over time.¹³ Microvascular density measurements have been performed on histological sections of vascular tissue using both manual^{15,16} and semiautomated

techniques.^{17–19} The ability to image and assess these same microvascular structures *in vivo* offers the potential for earlier detection and serial examinations of cardiovascular and retinal disease.

Studies of the foveal microvasculature using intravenous fluorescein angiography (FA)²⁰ have shown enlargement of the foveal avascular zone (FAZ) and perifoveal intercapillary areas in different disease states, including diabetes, hypertension, venous occlusion, glaucoma, and sickle cell disease.^{21–27} The ability to directly quantify microvascular density, however, has been limited by the eye's natural optical aberrations and the resolution of available ophthalmoscopes.^{15,28} More modern

TABLE. Demographic of Subjects With Retinal Vasculopathy

Subject	Age, y	Sex	Past Medical History	Medications	Past Ophthalmic History	Treatment History	Imaged Eye	BCVA
RR_0129	55	F	HTN, hyperlipidemia	Losartan, simvastatin, furosemide	Superior temporal BRVO OS	Laser photocoagulation ×2	OS	20/20-2
RR_0151	64	F	Bipolar disorder	Valproic acid, risperidone	Nonischemic CRVO OS	Intravitreal bevacizumab injection ×8	OS	20/20
RR_0167	49	F	DM ×12 y	Sitagliptin metformin	PDR OU ×2 y	Intravitreal bevacizumab injection ×2	OS	20/20
RR_0204	44	F	Sickle cell disease, pain crises	None	SCR OU	Laser photocoagulation ×6	OD	20/32
RR_0282	50	M	Hyperlipidemia	Simvastatin	BRAO OD	None	OD	20/20
RR_0332	70	M	HTN	None	HR OU	None	OS	20/40

F, female; M, male; HTN, hypertension; DM, diabetes mellitus.

ophthalmoscopes, such as adaptive optics (AO) scanning light ophthalmoscope (SLO),²⁹⁻³² optical coherence tomography (OCT),³³⁻³⁸ AO-OCT,³⁹ and AO flood-illumination,⁴⁰⁻⁴² allow more direct in vivo assessment of the retinal microvasculature. Adaptive optics ophthalmoscopy offers the greatest in vivo resolution and has been used to obtain capillary densities in both normal⁴³ and diabetic eyes.^{44,45}

We recently demonstrated that successful two-dimensional in vivo imaging of normal and diseased human microvasculature can be performed using AOSLO FA.⁴⁶⁻⁴⁸ In the present manuscript, we introduce analytic methods to study AOSLO FA images of the foveal microvasculature. We apply these methods to healthy young adult eyes and a representative group of vasculopathic eyes.

METHODS

Patient Recruitment

This study followed the tenets of the Declaration of Helsinki and was approved by the New York Eye and Ear Infirmary Institutional Review Board. Written informed consent was obtained from each participant after the nature and potential risks of the study were explained. Inclusion criteria included a best-corrected visual acuity (BCVA) of 20/60 or more with good central fixation, pupil dilation of at least 5 mm, normal anterior segment with clear phakic lens, clear media, and minimal or no inner retinal edema at the fovea on spectral-domain OCT (SD-OCT) (Heidelberg Spectralis HRA+OCT; Heidelberg Engineering, Inc., Heidelberg, Germany). Sixteen healthy adults (26 eyes) and six patients with a known retinal vasculopathy (six eyes) were enrolled.

The 16 healthy adults included eight men and eight women with a mean age of 25 years (range, 21-29). They had no significant past medical or surgical history with normal ocular examination and a BCVA of 20/20 or more in each study eye. Both eyes were imaged in 10 healthy adults, with only one eye imaged in the remaining six. The six patients with retinal vasculopathies included two men and four women with a mean age of 55 years (range, 44-70). One eye from each of the patients with vasculopathy was imaged. The BCVA was 20/40 or more in each eye and diagnoses included proliferative diabetic retinopathy (PDR), hypertensive retinopathy (HR), sickle cell retinopathy (SCR), nonischemic central retinal vein occlusion (CRVO), branch retinal vein occlusion (BRVO), and branch retinal artery occlusion (BRAO) (Table).

Imaging

Mydriasis and cycloplegia were achieved with one drop each 2.5% phenylephrine hydrochloride ophthalmic solution

(Bausch & Lomb, Inc., Tampa, FL, USA) and 1% tropicamide ophthalmic solution (Akorn, Inc., Lake Forest, IL, USA). Spectral-domain OCT imaging was performed on both eyes of all subjects, using 12 radial scans at 15° intervals through the center of the fovea. Each scan spanned 20° and was an average of nine frames. Axial length was measured in all eyes (IOL Master; Carl Zeiss Meditec AG, Jena, Germany) to calculate the AOSLO image scale in microns per pixel, based on the Emsley schematic eye model.⁴⁹

The AOSLO used was a replica of the one built by Dubra and Sulai,⁵⁰ modified for AOSLO FA as described by Pinhas et al.⁴⁶ The infrared (IR) reflectance channel used a 790-nm light, and the fluorescence channel used a 488-nm light for excitation and an emission filter centered at 525 nm with a 45-nm bandwidth. The fluorescence channel was focused on the superficial layers of retinal microvasculature, and the IR reflectance channel was focused on the photoreceptors. Fluorescein was administered orally in orange juice 10 to 20 minutes before AOSLO imaging at dosages of 20 mg fluorescein/kg body weight. During AOSLO FA, simultaneous 1.75° field-of-view reflectance and fluorescence image sequences 500 frames long were acquired at a rate of 15 frames per second. During recording of the 500-frame sequences, the internal fixation target was moved at 1.5° increments every 100 to 150 frames to image a contiguous square area of approximately 6° centered at the fovea. An additional set of images using only the IR channel focused on the superficial microvasculature was acquired, covering a square area of approximately 2.5° centered at the fovea, for comparison with FA perfusion maps. During imaging, subjects were given periodic short breaks as needed.

Light Safety

The AOSLO optical powers without modulation measured at the cornea were 15 μW for the 850-nm wavefront sensing superluminescent diode (SLD), 100 μW for the 790-nm imaging SLD, and 32 μW for the 488-nm diode laser. During imaging, the on/off modulation reduced the average powers delivered to approximately 25% of their original values. In imaging contiguous areas, no single retinal location was exposed to the combined light sources for longer than 30 seconds. All sources were considered lasers for the maximum permissible exposure (MPE) calculations, resulting in light exposure six times below both the photochemical and thermal MPE limits according to the American National Standards Institute ANSI Z136.⁵¹

Image Processing

After AOSLO FA imaging, both the reflectance (IR structural) and fluorescence (FA perfusion) sequences were registered

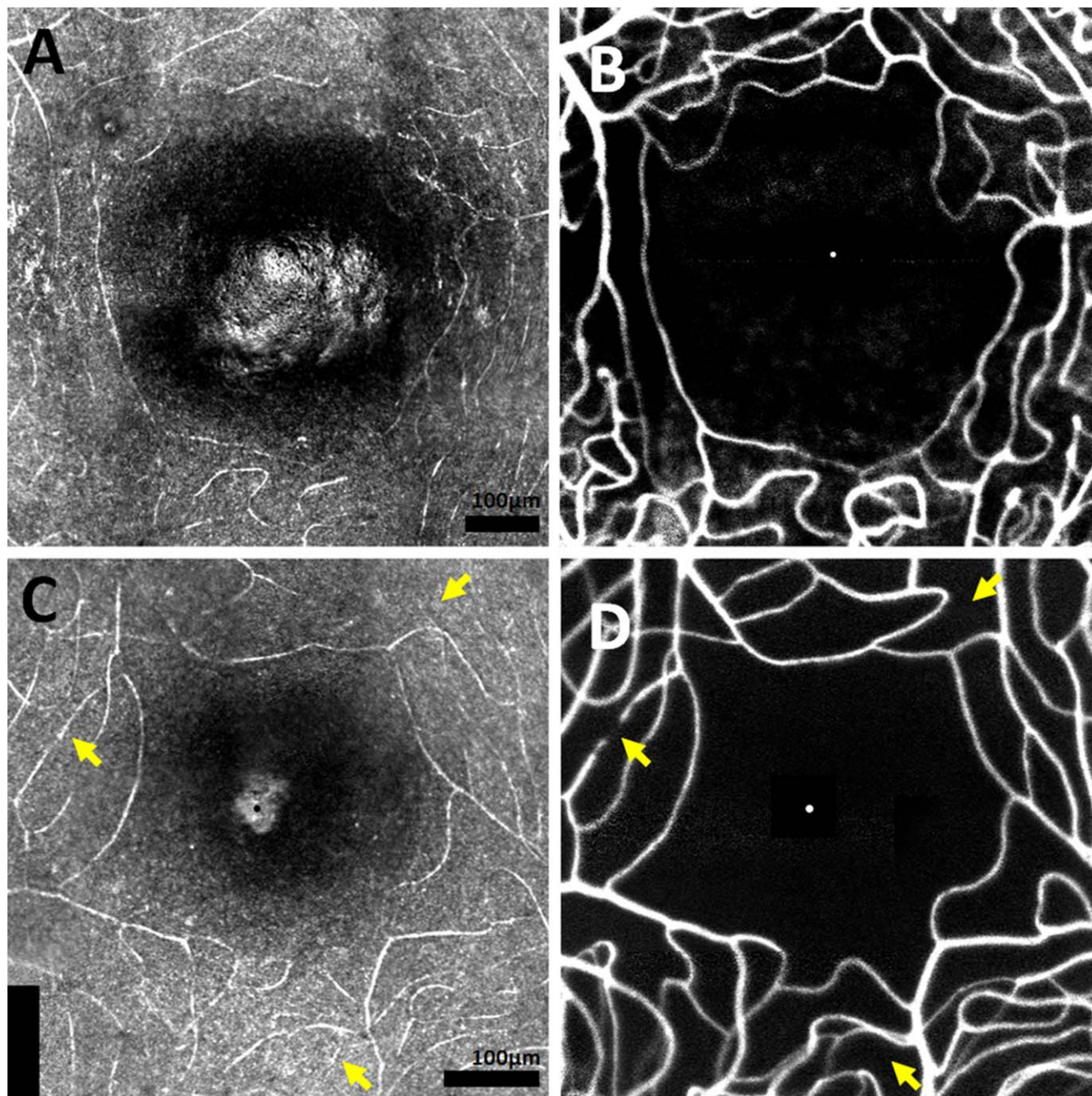


FIGURE 1. In the first example of a healthy 25-year-old male RR_0025 OS, comparing (A) IR structural map of FAZ and surrounding capillaries to the corresponding (B) FA perfusion map does not reveal nonperfused capillaries. In the second example of a 24-year-old male RR_0283 OS, at least three nonperfused capillaries are apparent (*arrows*). (A, C): The foveal center was identified in each IR structural map as the brightest point of the foveal reflex. Supplementary Video S1 shows registered FA perfusion and IR structural movies, with an *arrow* indicating a nonperfused capillary inferior to the FAZ. Scale bar: 25 μm (Supplementary Video S1).

using custom software,⁵² creating sequences with 5 to 100 frames. Images with high signal-to-noise ratio were generated by averaging the registered sequences. The individual microvascular IR structural and FA perfusion images were tiled manually and contrast stretched to create larger microvascular maps (Adobe Photoshop CS6; Adobe Systems, Inc., San Jose, CA, USA) (Figs. 1A, 1B).

Image Analysis

Detection of Nonperfused Capillaries. Infrared structural maps allowed visualization of the superficial capillaries,

irrespective of their perfusion status, whereas FA perfusion maps allowed visualization of only the perfused intraluminal spaces. By comparing the IR structural maps with the FA perfusion maps, it was possible to use any discrepancies to detect nonperfused capillaries adjacent to the FAZ (Fig. 1). Fluorescein angiography perfusion maps were also inspected for classic signs of microangiopathy, such as microaneurysms and/or vessel looping.

Microvascular Density Estimation. Circular FA perfusion maps centered at the fovea with a radius of 800 μm were analyzed using a custom-developed MATLAB GUI program (The

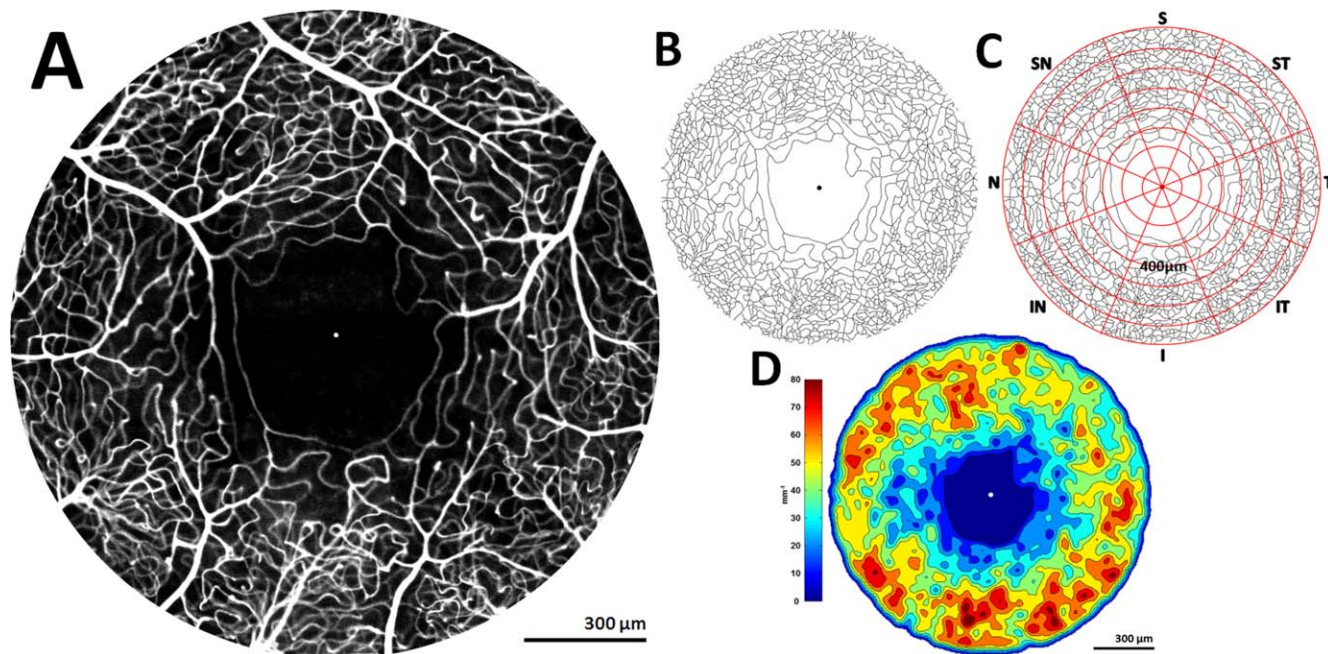


FIGURE 2. (A) Fluorescein angiography perfusion map of healthy 25-year-old male RR_0025 OS, 1600 μm in diameter, with *dot* marking foveal center. (B) Skeletonized perfusion maps were created by semiautomated tracing and (C) overlaid by a grid of 64 ROIs defined by eight equiangular octants and eight concentric annuli with a 100- μm step size. (D) Colorized density contour maps were created from skeletonized perfusion maps to visualize regional variation in microvascular topography.

Mathworks, Inc., Natick, MA, USA; Fig. 2A). The foveal center on each IR structural map was identified as the point of the maximum foveal reflex (Figs. 1A, 1C). With the approximate foveal center marked, each perfusion map was thresholded into a binary image. A skeletonized perfusion map was created in a semiautomated fashion. An automated skeletonization was first performed using single-pixel centerline extraction of the binary blood vessel maps, reducing all vascular structure to a single-pixel thickness, ignoring variations in vessel caliber and shape (Fig. 2B). The automated skeletonization was then manually corrected by erasing erroneous nonvascular features and tracing missed blood vessels. Interobserver reliability for vessel tracing was assessed by having two trained, independent examiners manually correct the automated skeletonization of a $200 \times 200\text{-}\mu\text{m}$ square region centered at 600 μm superior from the foveal center in each of the 16 healthy eyes. Intraclass correlation of their resulting microvascular density values was calculated.

Concentric circles centered at the fovea were generated at 100- μm radial increments over the finalized skeletonized perfusion map, creating a set of concentric annuli centered at the fovea. For example, annulus 200 represented the area between 100 and 200 μm radially from the foveal center. Eight equiangular radial lines emanating from the foveal center were also generated, creating octants: superior (S), superior nasal (SN), nasal (N), inferior nasal (IN), inferior (I), inferior temporal (IT), temporal (T), and superior temporal (ST). The confluence of circular and radial lines created 64 individual regions of interest (ROIs) (Fig. 2C). Microvascular density (mm^{-1}) was calculated by summing all the skeleton pixels within a given ROI, converting to millimeters using axial length correction,⁴⁹ and then dividing by the area of the ROI in millimeters squared. Individual ROI microvascular densities were grouped into annulus and octant means for further analysis. In calculating mean microvascular densities per eye, the central 400 μm were excluded to avoid the effect of

substantial FAZ diameter variation across individuals. These means were then averaged, and SD was calculated for those group averages. An unpaired *t*-test with a *P* value of less than 0.05 was used to measure significant difference between-group averages.

A separate algorithm created colorized density contour maps by computing microvascular density within each $16 \times 16\text{-}\mu\text{m}$ sampling window with 8- μm overlaps over the skeletonized perfusion maps using the built-in MATLAB function `blkproc`. Colorized density contour maps allowed for better visualization of regional vessel density variations across the FA perfusion map (Fig. 2D).

Spectral-Domain OCT Manual Segmentation and Analysis. Manual segmentation of 12 SD-OCT radial scans was performed for each eye, using a custom MATLAB GUI program. The inner limiting membrane (ILM), outer plexiform layer/outer nuclear layer interface (OPL/ONL), and the retinal pigment epithelium/choroid interface (RPE/CH) were segmented to define the inner retinal thickness (IRT) between ILM and OPL/ONL and outer retinal thickness (ORT) between OPL/ONL and RPE/CH. Data points were collected from 50- to 750- μm radial distance from foveal center in both directions per radial scan, to correspond to vessel density averages. This resulted in 24 data points per octant and 24 data points per annulus. Mean IRT and ORT per annulus and per octant were trended with respective microvascular density averages of the 16 healthy control eyes.

RESULTS

Analysis of healthy eye data included 16 nonfellow eyes of the 16 different healthy subjects. Use of data from the 10 healthy fellow eyes was limited to intrasubject difference calculations. Fluorescein angiography perfusion maps enhanced the visualization of the perfused foveal microvasculature. Fluorescein angiography perfusion maps of vasculopathic eyes showed

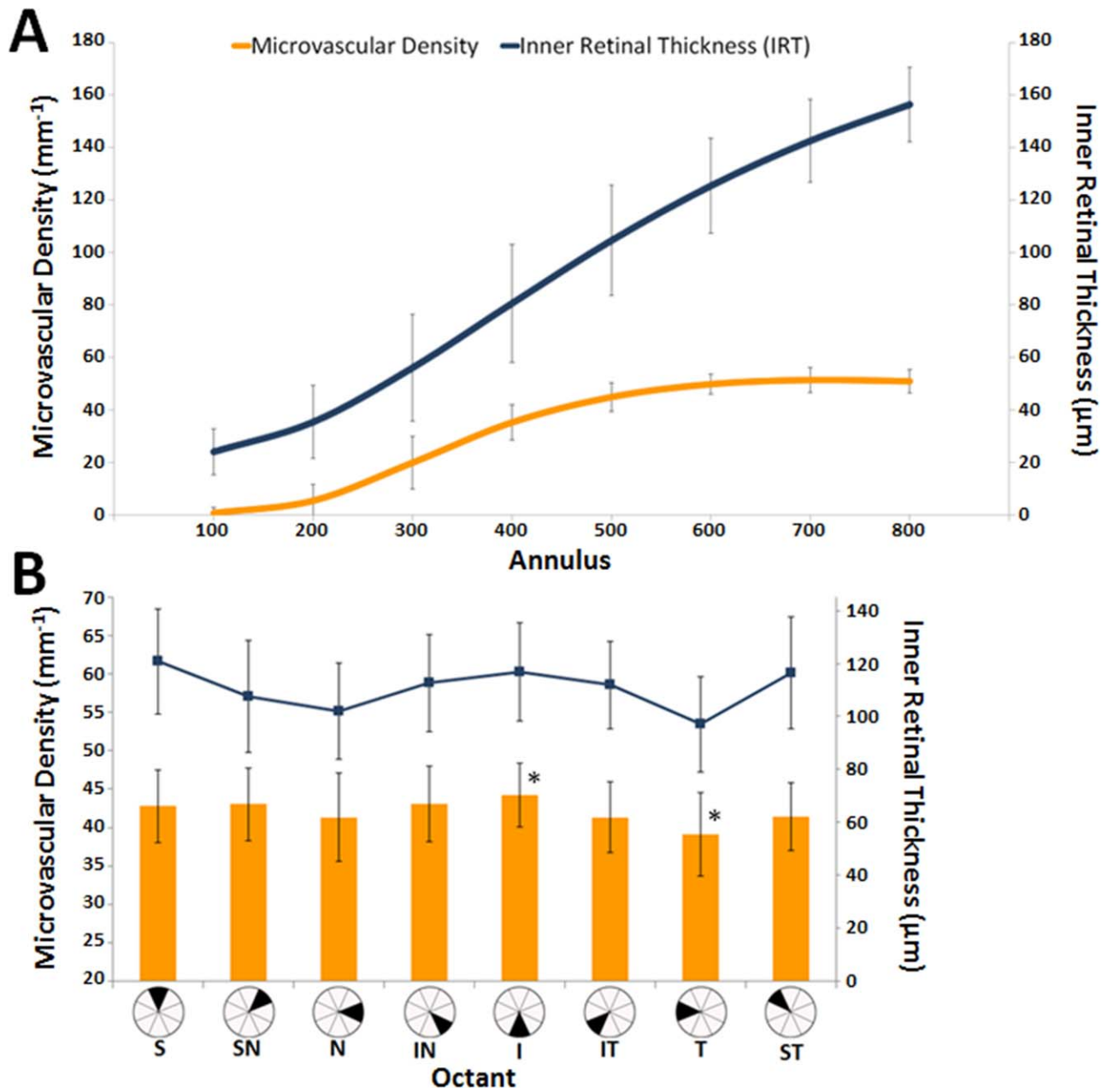


FIGURE 3. (A) An annulus comparison of average microvascular densities and respective average IRTs. (B) Microvascular density comparison by octant. Error bars represent SD. The asterisks represent a significant difference in microvascular density between the inferior and temporal octants.

subjectively lower microvascular density and larger FAZs compared with that of healthy controls, as well as microvascular looping and microaneurysms of various shapes and sizes. Comparison of IR structural and FA perfusion maps revealed nonperfused capillaries near the FAZ (Fig. 1; Supplementary Video S1). We were able to identify at least one nonperfused capillary segment in five (31%) of the 16 healthy nonfellow eyes and in four (66%) of the six vasculopathic eyes (BRVO, CRVO, PDR, and SCR). Capillary nonperfusion in vasculopathic eyes was more extensive compared with healthy eyes.

Interobserver vessel tracing reliability among the two readers was high (intraclass correlation coefficient 0.96). Average microvascular density of the 16 healthy nonfellow eyes was $42.0 \pm 4.2 \text{ mm}^{-1}$ (SD), with a range of 33.0 to 50.0 mm^{-1} . Microvascular densities increased along radial eccentricity from the foveal center (Fig. 3A). Superior and inferior

octants had higher microvascular densities compared with the nasal and temporal octants. There was a significant difference between the inferior and temporal octants ($44.0 \pm 4.2 \text{ mm}^{-1}$ versus $39.0 \pm 5.4 \text{ mm}^{-1}$; $t(14) = 4.4$, $P < 0.001$ (Fig. 3B). Average microvascular density was significantly higher in males versus females; $45.0 \pm 3.0 \text{ mm}^{-1}$ vs. $40.0 \pm 2.0 \text{ mm}^{-1}$; $t(14) = 3.0$, $P < 0.01$. The 10 healthy paired eyes showed no significant intrasubject differences in microvascular densities ($t[8] = 0.55$, $P = 0.60$) with percentage differences between OD and OS of 10% or less for all pairs.

Microvascular density increased along with IRT until depths of approximately 100 μm were reached (Fig. 3A). Inner retinal thickness values paralleled microvascular density variations across the octants, with superior and inferior octants showing higher thicknesses and nasal and temporal octants showing lower thicknesses (Fig. 3B). Outer retinal thickness values

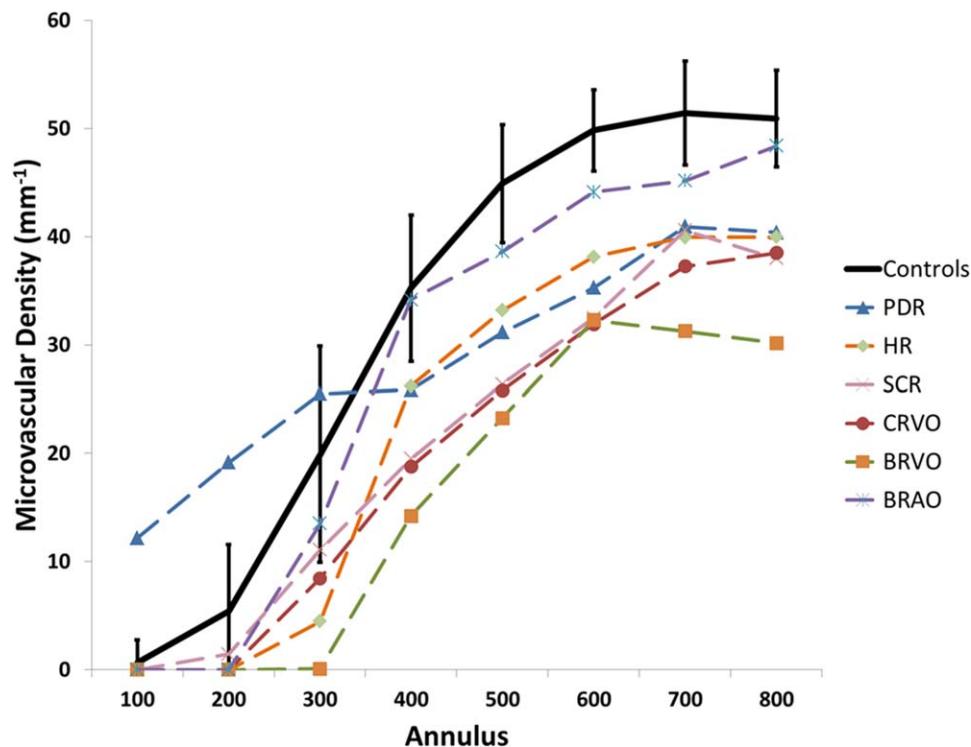


FIGURE 4. Microvascular density means per annulus of six vasculopathic eyes, compared with average microvascular density \pm SD of the 16 healthy nonfellow eyes. Vasculopathic eyes generally had lower microvascular densities compared with healthy averages. The PDR eye showed increased microvascular density from annulus 100 to 300 compared with healthy averages.

remained relatively constant compared with microvascular density variations across all octants and annuli. All six vasculopathic eyes had decreased microvascular densities when compared with controls (Fig. 4). Figures 5 and 6 show FA perfusion maps and corresponding colorized density contour maps of six representative healthy eyes and six vasculopathic eyes, respectively. For an IR structural and FA perfusion map comparison example of RR_0167 PDR OS, please refer to Figures 6C and 6D of Dubow et al.⁴⁷

DISCUSSION

Adaptive optics SLO confocal IR reflectance imaging and FA appear useful for evaluating the integrity of foveal microvascular features, and are sensitive enough to identify capillary nonperfusion as focal as a single capillary segment. Comparison of IR structural maps and FA perfusion maps revealed that even in young healthy eyes, there is a relatively common incidence of nonperfused capillaries near the FAZ (5 of 16 healthy eyes, or 31%). This finding may be normal variation and represent a dynamic process of functional nonperfusion/reperfusion, or may indicate the early stage of subclinical pathology. Future longitudinal imaging studies of these nonperfused capillary segments in healthy eyes may elucidate these findings. In an effort to minimize incoming light from nonvascular structures and better visualize the vascular structures on IR structural maps, techniques using multiply scattered light detection schemes, such as offset pinhole^{30,32} and split detection,⁵³ may be used.

In our limited sample of control subjects, we found a high degree of variation in microvascular densities between individuals (range, 33–50 mm^{-1}) with a low degree of variation between fellow eyes. This is most likely related to both genetic

and environmental factors between individuals. Our data also show that octant and annular microvascular densities increased along with increasing IRT on SD-OCT, whereas ORT values remained constant and did not appear to correlate with changes in microvascular density. These results are consistent with the known relationship between retinal vascular supply and the inner retinal tissue, as opposed to the outer retinal tissues that are supplied with oxygen by the choroidal vasculature.⁵⁴ We also found significant differences between male and female microvascular densities. However, there was a scarcity of available data in the literature to compare to our own with the exception of studies of vessel caliber and macular thickness. Population-based studies of vessel caliber have not found sex differences.^{55–57} A number of SD-OCT studies have found that males have significantly thicker maculae compared with females.^{58–62} Future studies will need to further explore the relationships among sex, anatomic structure, and microvascular density.

A number of groups have recently reported efforts to quantify retinal microvascular density. Using AOSLO motion contrast techniques, Tam et al.²⁹ showed that average vessel density in 15 normal eyes from the FAZ edge to 0.15° from the FAZ edge (approximately 317–370- μm radial distance from the foveal center) was 32 mm^{-1} . A comparable annulus in our study was annulus 400 (300–400- μm radial distance from the foveal center) in which average vessel density was 35 mm^{-1} . Using dual-conjugate AO, Popovic et al.⁴³ showed that average vessel density in five normal eyes from the FAZ edge (approximately 306- μm radial distance from the foveal center) to 750- μm radial distance from the foveal center was 37 mm^{-1} . A comparable range in our study was annuli 400 to 800, for which the average vessel density was 46 mm^{-1} . Both Tam et al.²⁹ and Popovic et al.⁴³ used methods similar to single-pixel

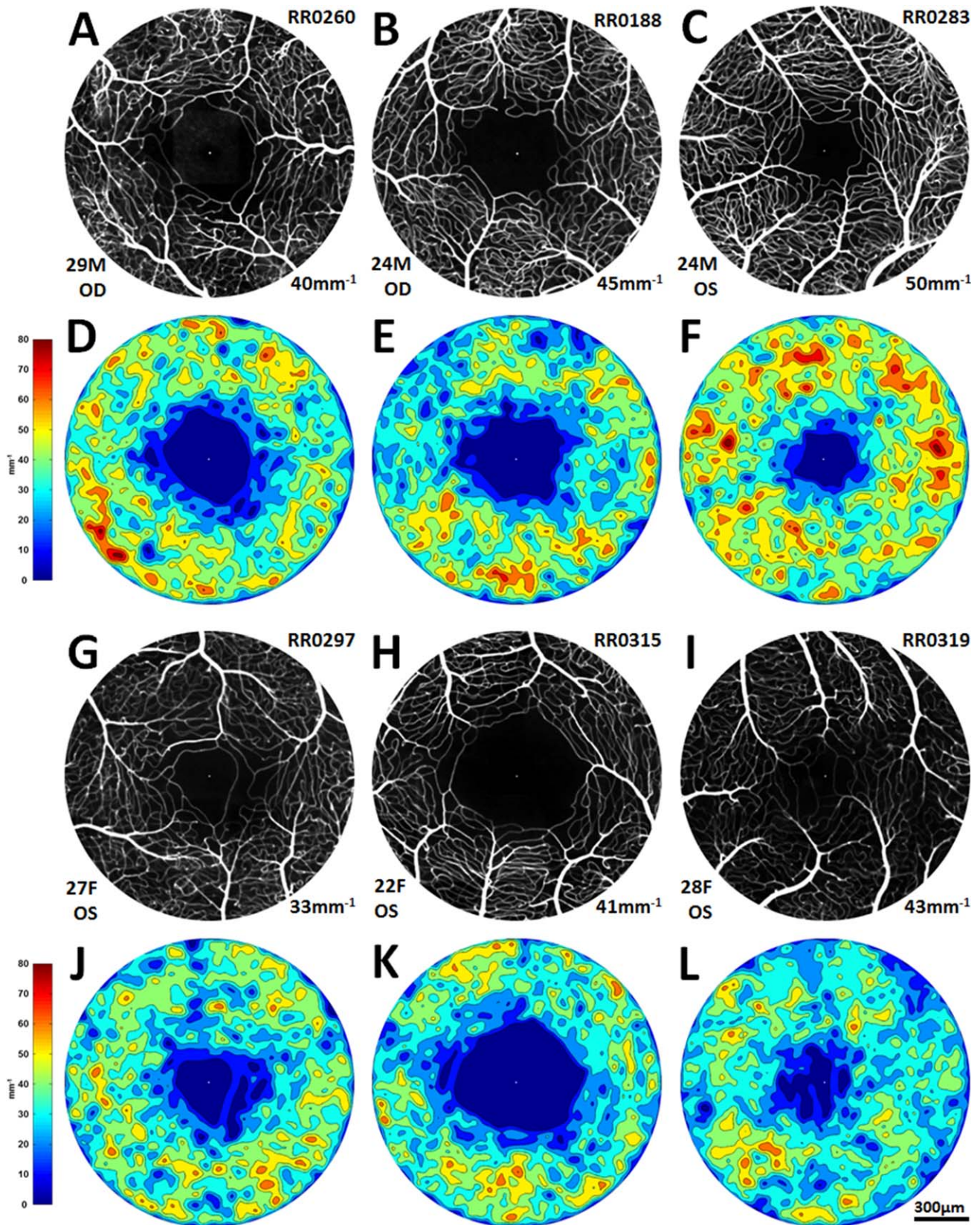


FIGURE 5. (A–C, G–I): Six representative healthy FA perfusion maps, three males and three females, showing a spectrum of FAZ shapes and sizes and a spectrum of microvascular densities. Subject identification number appears in the *upper right corner*; age, sex, and eye in the *lower left corner*; and microvascular density (mean of annuli 300–800) in the *lower right corner*. (D–F, J–L): Corresponding colorized density contour maps.

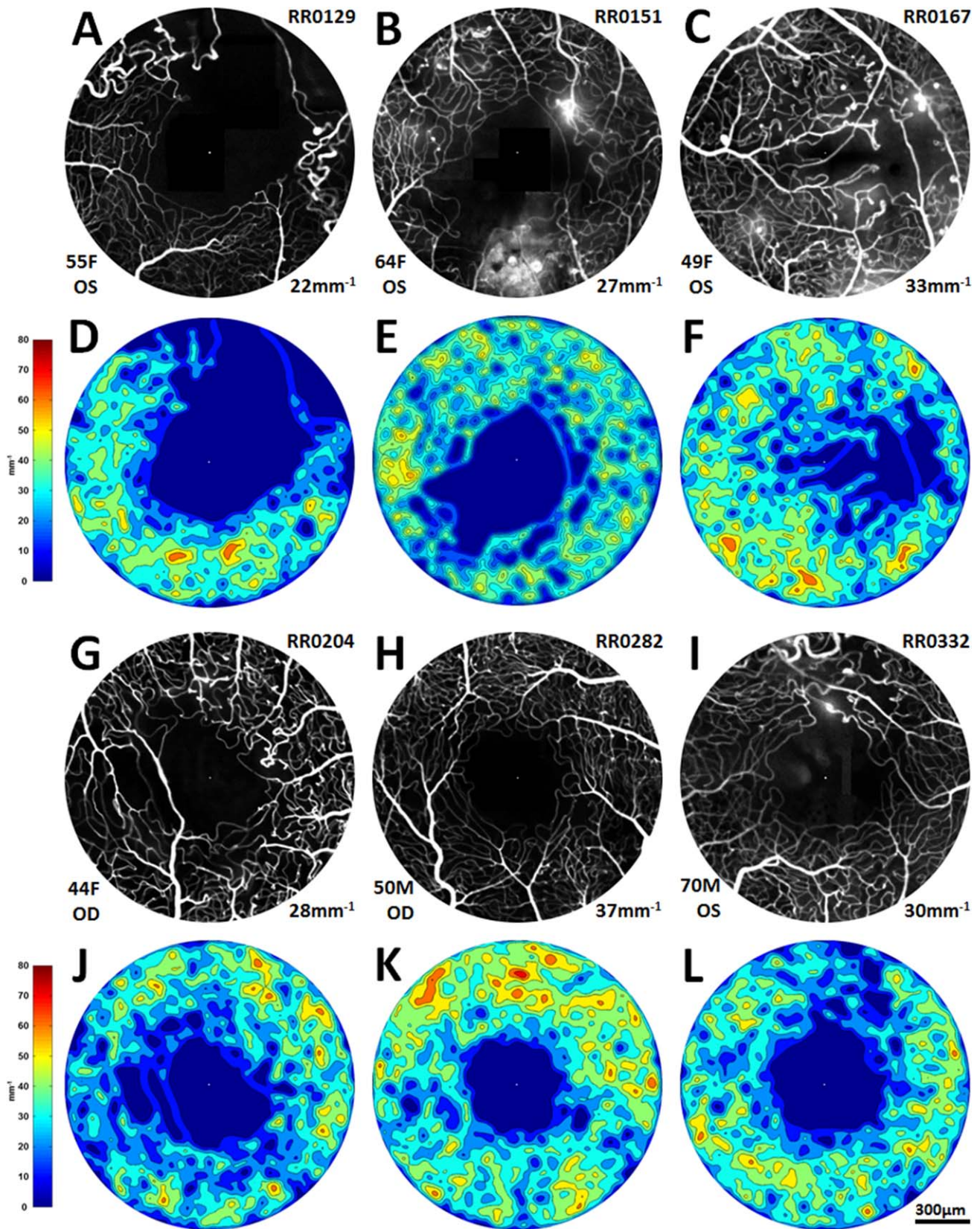


FIGURE 6. (A–C, G–I): Fluorescein angiography perfusion maps of the six vasculopathic eyes, in order of appearance: BRVO, CRVO, PDR, SCR, BRAO, and HR. Subject identification number appears in the *upper right corner*; age, sex, and eye in the *lower left corner*; and microvascular density (mean of annuli 300–800) in the *lower right corner*. (D–F, J–L): Corresponding colorized density contour maps.

centerline extraction. The higher microvascular density of AOSLO FA compared with reflectance AO techniques may in part be due to its ability to image more microvascular layers at a given axial focus.⁴⁸

Mendis et al.¹⁵ and Chan et al.¹⁶ independently reported on histologic microvascular densities using confocal microscopy. Both defined vessel density as the percentage of the image occupied by retinal vessels, and moved the focus to image different microvascular layers. Mendis et al.¹⁵ showed that in five donor eyes, average vessel density at two $1300 \times 1300\text{-}\mu\text{m}$ regions, from $850 \mu\text{m}$ to $2150 \mu\text{m}$ temporally and inferiorly from the foveal center, was 64.1%. Chan et al.¹⁶ showed that in 11 donor eyes, average vessel density at a $500 \times 500\text{-}\mu\text{m}$ region centered 2 mm from the foveal center was 77.2%. These data are somewhat difficult to compare with our own because the analyzed regions were farther from the foveal center and the density calculations incorporated vascular caliber. Additionally, our method was limited to a single superficial focal depth, which may have ignored deeper microvascular layers. Figure 3A shows that at an IRT of approximately $100 \mu\text{m}$, microvascular density begins to approach an apparent asymptote, whereas IRT continues to increase with increasing distance from the foveal center. The relationship of microvascular density and IRT beyond a depth of $100 \mu\text{m}$ is nonphysiologic and more likely represents the limit of the current AOSLO FA method (e.g., imaging wavelength, power, pinhole size) in imaging deeper microvascular layers while focused at the superficial microvasculature. That being said, our annulus 800 average microvascular density of 51mm^{-1} indicates that our *in vivo* technique is able to capture the bulk of the microvasculature present in the retinal tissue. In future studies, modification of settings may facilitate imaging at eccentricities beyond annulus 800 and use multiple foci to produce results more comparable with those histological studies of Mendis et al.¹⁵ and Chan et al.¹⁶

An additional limitation of the current study was the lack of age-matched healthy eyes for comparison with vasculopathic eyes. The vasculopathic subjects in this study were older than the healthy subjects, and it is not possible to rule out that at least some of the changes observed in capillary nonperfusion and microvascular density may have been age-related. The procedure of identifying the foveal center is another possible confounding feature of this study. Choosing the brightest point of the foveal reflex on the IR structural maps may have introduced a source of error into microvascular density calculations. We chose not to calculate the center of FAZ using the capillaries that encircle the FAZ, because in disease states dropout surrounding FAZ may occur asymmetrically. The significance of this possible source of error needs to be further investigated by cross-referencing the foveal reflexes on IR structural maps with the point of highest cone density on IR photoreceptor images and foveal pit morphology on SD-OCT scans. Another limitation of this study is that diseased or aged vessels may be more reflective secondary to sclerosis, which can potentially make them more readily identifiable on IR structural maps compared with healthy vessels. Identification of nonperfusion in healthy vessels may thus be more difficult when compared with that in diseased or aged vessels, affecting relative calculated rates of nonperfusion across the groups.

The preliminary normative and select vasculopathy database presented in this study suggests that simultaneous AOSLO confocal IR reflectance and fluorescence imaging have the potential to help better characterize normal microvasculature versus age-related change, retinal vasculopathy, or systemic cardiovascular disease. Furthermore, AOSLO FA has potential to reveal tissue response to current and emerging treatment modalities, and may aid in the discovery and development of novel treatment options. Improvements in image acquisition,

processing, and analysis are required before this technique can successfully integrate into a clinical setting. Its potential as a tool for tracking disease state and correlating with other imaging modalities, such as SD-OCT, blood flow,⁶³⁻⁶⁵ microperimetry,⁶⁶ and metabolic imaging,⁶⁷ may help detect disease earlier, prognosticate more accurately, and point the way toward more personalized management of disease.

Acknowledgments

The authors thank Eric Cheang, Chun Lin Liu, and Lenny Rostomian for their assistance with image processing.

Supported by the Marrus Family Foundation, Bendheim-Lowenstein Family Foundation, Wise Family Foundation, R.D. and Linda Peters Foundation, Edith C. Blum Foundation, Chairman's Research Fund of the New York Eye and Ear Infirmary of Mount Sinai, the Glaucoma Research Foundation, an unrestricted departmental grant from Research to Prevent Blindness, National Institutes of Health grants P30EY001931 and UL1TR000055, and a Career Development Award from Research to Prevent Blindness and a Career Award at the Scientific Interface from the Burroughs Wellcome Fund (AD).

Disclosure: **A. Pinhas**, None; **M. Razeen**, None; **M. Dubow**, None; **A. Gan**, None; **T.Y. Chui**, None; **N. Shah**, None; **M. Mehta**, None; **R.C. Gentile**, None; **R. Weitz**, None; **J.B. Walsh**, None; **Y.N. Sulai**, None; **J. Carroll**, None; **A. Dubra**, P; **R.B. Rosen**, Clarity (C); OD-OS (C); Optovue (C); Allergan (C); Advanced Cell Technologies (C), P

References

1. Kawasaki R, Xie J, Cheung N, et al. Retinal microvascular signs and risk of stroke: the Multi-Ethnic Study of Atherosclerosis (MESA). *Stroke*. 2012;43:3245-3251.
2. Hanff TC, Sharrett AR, Mosley TH, et al. Retinal microvascular abnormalities predict progression of brain microvascular disease: an atherosclerosis risk in communities magnetic resonance imaging study. *Stroke*. 2014;45:1012-1017.
3. Heringa SM, Bouvy WH, van den Berg E, Moll AC, Kappelle LJ, Biessels GJ. Associations between retinal microvascular changes and dementia, cognitive functioning, and brain imaging abnormalities: a systematic review. *J Cereb Blood Flow Metab*. 2013;33:983-995.
4. Tabatabaee A, Asharin MR, Dehghan MH, Pourbehi MR, Nasiri-Ahmadabadi M, Assadi M. Retinal vessel abnormalities predict coronary artery diseases. *Perfusion*. 2013;28:232-237.
5. Lim IS, Cheung CY, Sabanayagam C, et al. Structural changes in the retinal microvasculature and renal function. *Invest Ophthalmol Vis Sci*. 2013;54:2970-2976.
6. Liew G, Wong TY, Mitchell P, Newall P, Smith W, Wang JJ. Retinal microvascular abnormalities and age-related hearing loss: the Blue Mountains hearing study. *Ear Hear*. 2007;28:394-401.
7. Frank RN. Diabetic retinopathy. *N Engl J Med*. 2004;350:48-58.
8. Kim SY, Johnson MA, McLeod DS, Alexander T, Hansen BC, Luttly GA. Neutrophils are associated with capillary closure in spontaneously diabetic monkey retinas. *Diabetes*. 2005;54:1534-1542.
9. Durham JT, Herman IM. Microvascular modifications in diabetic retinopathy. *Curr Diab Rep*. 2011;11:253-264.
10. Vicaut E. Hypertension and the microcirculation: a brief overview of experimental studies. *J Hypertens Suppl*. 1992;10:S59-S68.
11. Huang SS, Khosrof SA, Koletsky RJ, Benetz BA, Ernsberger P. Characterization of retinal vascular abnormalities in lean and obese spontaneously hypertensive rats. *Clin Exp Pharmacol Physiol Suppl*. 1995;22:S129-S131.

12. Buchi ER, Kurosawa A, Tso MO. Retinopathy in diabetic hypertensive monkeys: a pathologic study. *Graefes Arch Clin Exp Ophthalmol*. 1996;234:388-398.
13. Levy BI, Schiffrin EL, Mourad JJ, et al. Impaired tissue perfusion: a pathology common to hypertension, obesity, and diabetes mellitus. *Circulation*. 2008;118:968-976.
14. Manwani D, Frenette PS. Vaso-occlusion in sickle cell disease: pathophysiology and novel targeted therapies. *Hematology Am Soc Hematol Educ Program*. 2013;2013:362-369.
15. Mendis KR, Balaratnasingam C, Yu P, et al. Correlation of histologic and clinical images to determine the diagnostic value of fluorescein angiography for studying retinal capillary detail. *Invest Ophthalmol Vis Sci*. 2010;51:5864-5869.
16. Chan G, Balaratnasingam C, Yu PK, et al. Quantitative morphometry of perifoveal capillary networks in the human retina. *Invest Ophthalmol Vis Sci*. 2012;53:5502-5514.
17. Vickerman MB, Keith PA, McKay TL, et al. VESGEN 2D: automated, user-interactive software for quantification and mapping of angiogenic and lymphangiogenic trees and networks. *Anat Rec (Hoboken)*. 2009;292:320-332.
18. Zudaire E, Gambardella L, Kurcz C, Vermeren S. A computational tool for quantitative analysis of vascular networks. *PLoS One*. 2011;6:e27385.
19. Seaman ME, Peirce SM, Kelly K. Rapid analysis of vessel elements (RAVE): a tool for studying physiologic, pathologic and tumor angiogenesis. *PLoS One*. 2011;6:e20807.
20. Wykes WN, Livesey SJ. Review of fluorescein angiograms performed in one year. *Br J Ophthalmol*. 1991;75:398-400.
21. Arend O, Wolf S, Jung F, et al. Retinal microcirculation in patients with diabetes mellitus: dynamic and morphological analysis of perifoveal capillary network. *Br J Ophthalmol*. 1991;75:514-518.
22. Sander B, Larsen M, Engler C, Lund-Andersen H, Parving HH. Early changes in diabetic retinopathy: capillary loss and blood-retina barrier permeability in relation to metabolic control. *Acta Ophthalmol (Copenh)*. 1994;72:553-559.
23. Wolf S, Arend O, Schulte K, Ittel TH, Reim M. Quantification of retinal capillary density and flow velocity in patients with essential hypertension. *Hypertension*. 1994;23:464-467.
24. Parodi MB, Visintin F, Della Rupe P, Ravalico G. Foveal avascular zone in macular branch retinal vein occlusion. *Int Ophthalmol*. 1995;19:25-28.
25. Remky A, Wolf S, Knabben H, Arend O, Reim M. Perifoveal capillary network in patients with acute central retinal vein occlusion. *Ophthalmology*. 1997;104:33-37.
26. Sanders RJ, Brown GC, Rosenstein RB, Magargal L. Foveal avascular zone diameter and sickle cell disease. *Arch Ophthalmol*. 1991;109:812-815.
27. Arend O, Remky A, Plange N, Martin BJ, Harris A. Capillary density and retinal diameter measurements and their impact on altered retinal circulation in glaucoma: a digital fluorescein angiographic study. *Br J Ophthalmol*. 2002;86:429-433.
28. Weinhaus RS, Burke JM, Delori FC, Snodderly DM. Comparison of fluorescein angiography with microvascular anatomy of macaque retinas. *Exp Eye Res*. 1995;61:1-16.
29. Tam J, Martin JA, Roorda A. Noninvasive visualization and analysis of parafoveal capillaries in humans. *Invest Ophthalmol Vis Sci*. 2010;51:1691-1698.
30. Chui TY, Vannasdale DA, Burns SA. The use of forward scatter to improve retinal vascular imaging with an adaptive optics scanning laser ophthalmoscope. *Biomed Opt Express*. 2012;3:2537-2549.
31. Chui TY, Zhong Z, Song H, Burns SA. Foveal avascular zone and its relationship to foveal pit shape. *Optom Vis Sci*. 2012;89:602-610.
32. Chui TY, Gast TJ, Burns SA. Imaging of vascular wall fine structure in the human retina using adaptive optics scanning laser ophthalmoscopy. *Invest Ophthalmol Vis Sci*. 2013;54:7115-7124.
33. Srinivasan VJ, Adler DC, Chen Y, et al. Ultrahigh-speed optical coherence tomography for three-dimensional and en face imaging of the retina and optic nerve head. *Invest Ophthalmol Vis Sci*. 2008;49:5103-5110.
34. Schmoll T, Singh ASG, Blatter C, et al. Imaging of the parafoveal capillary network and its integrity analysis using fractal dimension. *Biomed Opt Express*. 2011;2:1159-1168.
35. Zhi Z, Yin X, Dziennis S, et al. Optical microangiography of retina and choroid and measurement of total retinal blood flow in mice. *Biomed Opt Express*. 2012;3:2976-2986.
36. Kim DY, Fingler J, Zawadzki RJ, et al. Noninvasive imaging of the foveal avascular zone with high-speed, phase-variance optical coherence tomography. *Invest Ophthalmol Vis Sci*. 2012;53:85-92.
37. Kim DY, Fingler J, Werner JS, Schwartz DM, Fraser SE, Zawadzki RJ. In vivo volumetric imaging of human retinal circulation with phase-variance optical coherence tomography. *Biomed Opt Express*. 2011;2:1504-1513.
38. Zotter S, Pircher M, Torzicky T, et al. Visualization of microvasculature by dual-beam phase-resolved Doppler optical coherence tomography. *Opt Express*. 2011;19:1217-1227.
39. Wang Q, Kocaoglu OP, Cense B, et al. Imaging retinal capillaries using ultrahigh-resolution optical coherence tomography and adaptive optics. *Invest Ophthalmol Vis Sci*. 2011;52:6292-6299.
40. Rha J, Jonnal RS, Thorn KE, Qu J, Zhang Y, Miller DT. Adaptive optics flood-illumination camera for high speed retinal imaging. *Opt Express*. 2006;14:4552-4569.
41. Lombardo M, Parravano M, Serrao S, Ducoli P, Stirpe M, Lombardo G. Analysis of retinal capillaries in patients with type 1 diabetes and nonproliferative diabetic retinopathy using adaptive optics imaging. *Retina*. 2013;33:1630-1639.
42. Bedggood P, Metha A. Direct visualization and characterization of erythrocyte flow in human retinal capillaries. *Biomed Opt Express*. 2012;3:3264-3277.
43. Popovic Z, Knutsson P, Thaug J, Owner-Petersen M, Sjostrand J. Noninvasive imaging of human foveal capillary network using dual-conjugate adaptive optics. *Invest Ophthalmol Vis Sci*. 2011;52:2649-2655.
44. Tam J, Dhamdhare KP, Tiruveedhula P, et al. Disruption of the retinal parafoveal capillary network in type 2 diabetes before the onset of diabetic retinopathy. *Invest Ophthalmol Vis Sci*. 2011;52:9257-9266.
45. Tam J, Dhamdhare KP, Tiruveedhula P, et al. Subclinical capillary changes in non-proliferative diabetic retinopathy. *Optom Vis Sci*. 2012;89:E692-E703.
46. Pinhas A, Dubow M, Shah N, et al. In vivo imaging of human retinal microvasculature using adaptive optics scanning light ophthalmoscope fluorescein angiography. *Biomed Opt Express*. 2013;4:1305-1317.
47. Dubow M, Pinhas A, Shah N, et al. Classification of human retinal microaneurysms using adaptive optics scanning light ophthalmoscope fluorescein angiography. *Invest Ophthalmol Vis Sci*. 2014;55:1299-1309.
48. Chui TY, Dubow M, Pinhas A, et al. Comparison of adaptive optics scanning light ophthalmoscopic fluorescein angiography and offset pinhole imaging. *Biomed Opt Express*. 2014;5:1173-1189.
49. Smith G, Atchison DA. *The Eye and Visual Optical Instruments*. 1st ed. Cambridge: Cambridge University Press; 1997.
50. Dubra A, Sulai Y. Reflective afocal broadband adaptive optics scanning ophthalmoscope. *Biomed Opt Express*. 2011;2:1757-1768.
51. Delori FC, Webb RH, Sliney DH. American National Standards I. Maximum permissible exposures for ocular safety (ANSI

- 2000), with emphasis on ophthalmic devices. *J Opt Soc Am A*. 2007;24:1250-1265.
52. Dubra A, Harvey Z. Registration of 2D images from fast scanning ophthalmic instruments. In: Fischer B, Dawant B, Lorenz C, eds. *Biomedical Image Registration*. Berlin: Springer; 2010:60-71.
 53. Sulai YN, Scoles D, Harvey Z, Dubra A. Visualization of retinal vascular structure and perfusion with a nonconfocal adaptive optics scanning light ophthalmoscope. *J Opt Soc Am A Opt Image Sci Vis*. 2014;31:569-579.
 54. Yu DY, Cringle SJ. Oxygen distribution and consumption within the retina in vascularised and avascular retinas and in animal models of retinal disease. *Prog Retin Eye Res*. 2001;20:175-208.
 55. Wong TY, Klein R, Klein BE, Meuer SM, Hubbard LD. Retinal vessel diameters and their associations with age and blood pressure. *Invest Ophthalmol Vis Sci*. 2003;44:4644-4650.
 56. Wang S, Xu L, Wang Y, Wang Y, Jonas JB. Retinal vessel diameter in normal and glaucomatous eyes: the Beijing eye study. *Clin Experiment Ophthalmol*. 2007;35:800-807.
 57. Cheung N, Islam FM, Saw SM, et al. Distribution and associations of retinal vascular caliber with ethnicity, gender, and birth parameters in young children. *Invest Ophthalmol Vis Sci*. 2007;48:1018-1024.
 58. Wong AC, Chan CW, Hui SP. Relationship of gender, body mass index, and axial length with central retinal thickness using optical coherence tomography. *Eye (Lond)*. 2005;19:292-297.
 59. Kelty PJ, Payne JF, Trivedi RH, Kelty J, Bowie EM, Burger BM. Macular thickness assessment in healthy eyes based on ethnicity using Stratus OCT optical coherence tomography. *Invest Ophthalmol Vis Sci*. 2008;49:2668-2672.
 60. Kashani AH, Zimmer-Galler IE, Shah SM, et al. Retinal thickness analysis by race, gender, and age using Stratus OCT. *Am J Ophthalmol*. 2010;149:496-502.
 61. Song WK, Lee SC, Lee ES, Kim CY, Kim SS. Macular thickness variations with sex, age, and axial length in healthy subjects: a spectral domain-optical coherence tomography study. *Invest Ophthalmol Vis Sci*. 2010;51:3913-3918.
 62. Wagner-Schuman M, Dubis AM, Nordgren RN, et al. Race- and sex-related differences in retinal thickness and foveal pit morphology. *Invest Ophthalmol Vis Sci*. 2011;52:625-634.
 63. Burgansky-Eliash Z, Nelson DA, Bar-Tal OP, Lowenstein A, Grinvald A, Barak A. Reduced retinal blood flow velocity in diabetic retinopathy. *Retina*. 2010;30:765-773.
 64. Burgansky-Eliash Z, Barak A, Barash H, et al. Increased retinal blood flow velocity in patients with early diabetes mellitus. *Retina*. 2012;32:112-119.
 65. Nelson DA, Burgansky-Eliash Z, Barash H, et al. High-resolution wide-field imaging of perfused capillaries without the use of contrast agent. *Clin Ophthalmol*. 2011;5:1095-1106.
 66. Winterhalter S, Lux A, Maier AK, et al. Microperimetry as a routine diagnostic test in the follow-up of retinal vein occlusion? *Graefes Arch Clin Exp Ophthalmol*. 2012;50:175-183.
 67. Elnor SG, Elnor VM, Field MG, Park S, Heckenlively JR, Petty HR. Retinal flavoprotein autofluorescence as a measure of retinal health. *Trans Am Ophthalmol Soc*. 2008;106:215-222; discussion 222-224.